Heliyon 9 (2023) e18708

Contents lists available at ScienceDirect

Heliyon

journal homepage: www.cell.com/heliyon

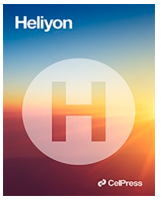

Identification and validation of a novel anoikis-related signature for predicting prognosis and immune landscape in ovarian serous cystadenocarcinoma

Yu-Ting Zhu [a,b,1], Shuang-Yue Wu [a,b,1], Song Yang [c,1], Jie Ying [a,b], Lu Tian [a,b], Hong-Liang Xu [d], He-Ping Zhang [d], Hui Yao [a,b], Wei-Yu Zhang [a,b], Qin-Qin Jin [a,b], Yin-Ting Yang [a,b], Xi-Ya Jiang [a,b], Nan Zhang [a,b], Shun Yao [a,b], Shu-Guang Zhou [a,b,**], Guo Chen [a,b,*]

[a] Department of Gynecology, Maternal and Child Health Hospital Affiliated to Anhui Medical University, Hefei, Anhui 230001, China
[b] Department of Gynecology, Anhui Province Maternity and Child Healthcare Hospital, Hefei, Anhui 230001, China
[c] Department of Pain Treatment, The First Affiliated Hospital of Anhui Medical University, Hefei, Anhui 230032, China
[d] Department of Pathology, Anhui Province Maternity and Child Healthcare Hospital, Hefei, Anhui 230001, China

ARTICLE INFO

Keywords:
Anoikis
Tumor metastasis
Ovarian serous cystadenocarcinoma
Prognosis
Immune landscape

ABSTRACT

Background: Ovarian serous cystadenocarcinoma (OSC) is the most prevalent histological subtype of ovarian cancer (OV) and presents a serious threat to women's health. Anoikis is an essential component of metastasis, and tumor cells can get beyond it to become viable. The impact of anoikis on OSC, however, has only been the topic of a few studies.
Methods: The mRNA sequencing and clinical information of OSC came from The Cancer Genome Atlas Target Genotype-Tissue Expression (TCGA TARGET GTEx) dataset. Anoikis-related genes (ARGs) were collected by Harmonizome and GeneCards websites. Centered on these ARGs, we used unsupervised consensus clustering to explore potential tumor typing and filtered hub ARGs to create a model of predictive signature for OSC patients. Furthermore, we presented clinical specialists with a novel nomogram based on ARGs, revealing the underlying clinical relevance of this signature. Finally, we explored the immune microenvironment among various risk groups.
Results: We identified 24 ARGs associated with the prognosis of OSC and classified OSC patients into three subtypes, and the subtype with the best prognosis was more enriched in immune-related pathways. Seven ARGs (ARHGEF7, NOTCH4, CASP2, SKP2, PAK4, LCK, CCDC80) were chosen to establish a risk model and a nomogram that can provide practical clinical decision support. Risk scores were found to be an independent and significant prognostic factor in OSC patients. The CIBERSORTx result revealed an inflammatory microenvironment is different for risk groups, and the proportion of immune infiltrates of Macrophages M1 is negatively correlated with risk score ($r_s = -0.21$, $P < 0.05$). Ultimately, quantitative reverse transcription polymerase chain reaction (RT-PCR) was utilized to validate the expression of the seven pivotal ARGs.

* Corresponding author. Department of Gynecology, Maternal and Child Health Hospital Affiliated to Anhui Medical University, Hefei, Anhui 230001, China.
** Corresponding author. Department of Gynecology, Maternal and Child Health Hospital Affiliated to Anhui Medical University, Hefei, Anhui 230001, China.
E-mail addresses: zhoushuguang@ahmu.edu.cn (S.-G. Zhou), chenguo@ahmu.edu.cn (G. Chen).
[1] These authors contributed equally.

https://doi.org/10.1016/j.heliyon.2023.e18708
Received 8 March 2023; Received in revised form 23 July 2023; Accepted 25 July 2023
Available online 26 July 2023

Conclusion: In this study, based on seven ARGs, a risk model and nomogram established can be used for risk stratification and prediction of survival outcomes in patients with OSC, providing a reliable reference for individualized therapy of OSC patients.

1. Introduction

OV is a female genital system malignancy associated with the highest mortality rate [1]. About 85%–90% of OV are of epithelial origin, with OSC being the most common histological type. With a lack of early typical symptoms, about 2/3 of OSC patients are diagnosed at stage III or IV [2], 5-year OS of only 42% and 26%, and invasion and migration are the main causes of its high mortality rate [3,4]. Hence, screening for new key molecules mediating ovarian cancer invasion and metastasis is essential for developing new treatment strategies.

Anoikis is a programmed death caused by losing contact between the extracellular matrix (ECM) and other cells, which is indispensable to maintaining homeostasis in the body. Its main role is to prevent cells from adhering to the abnormal ECM and growing abnormally [5]. Recent research has identified anoikis resistance as the bases for tumor cell metastasis [6,7]. The ability of tumor cells and associated endothelial cells to surmount anoikis and survive after detachment from the ECM has an important effect on tumor migration [8]. Research has demonstrated that the loss of apoptotic resistance is strongly linked to the metastatic invasion and prognosis of various tumor types, such as breast cancer [9], hepatocellular [10], and lung cancers [11]. However, studies on the impact of anoikis on OSC aggressiveness and their roles in predicting OSC prognosis are scarce.

In this study, we focus on the potential value of ARGs in forecasting prognosis in OSC and the construction of a model for prognosis. And investigate further the immune landscape between different risk classifications, which will facilitate individualized treatment of OSC patients.

2. Materials and methods

2.1. Downloading of data

Downloading the mRNA sequencing and clinical data of OSC patients in the TCGA TARGET GTEx dataset at UCSC Xena (http://xena.ucsc.edu). Aberrant expression values and deletions were removed by principal component analysis (PCA), resulting in 424 tumor samples and 88 normal samples. Moreover, the 424 OSC samples (TCGA-OV set) were randomly generated into 300 OSC samples (Test set) for internal validation. Furthermore, complete clinical information on the 424 OSC patients was downloaded from the TCGA database, including vital status, age, chemotherapy, grade, residue size, and so on. In addition, 734 anoikis-related genes (ARGs) were downloaded from GeneCards (https://www.genecards.org/) and Harmonizome (https://maayanlab.cloud/Harmonizome/).

2.2. Pre-processing of data

We performed a differential analysis of variance using the "limma" R package to screen differentially expressed genes (DEGs) that were aberrantly expressed in OSC and normal samples by a false discovery rate (FDR) < 0.05 and $|\log \text{fold change}|(|\log FC|) > 1$. Subsequently, 313 differentially expressed ARGs were filtered by intersecting DEGs with 734 ARGs. Finally, we obtained survival-associated ARGs via the “survival” R package.

2.3. Gene ontology (GO) enrichment analysis

We performed the “clusterProfiler” and "org.Hs.eg.db" R packages to analyze the GO functions of survival-associated ARGs. The GOChord function of the “Goplot” R package generated and visualized a circularly composited overview of the above ARGs and the top 10 assigned terms.

2.4. Consensus clustering

The "ConsensusClusterPlus" R package was available for differentiating samples into subtypes based on ARGs expression patterns via the k-means method [12]. Then, Stochastic Neighbor Embedding (*t*-SNE) and Uniform Manifold Approximation and Projection (UMAP) were employed, validating the accuracy of the clustering.

2.5. Gene set variation analysis (GSVA)

We were able to get "c2.cp. Kegg. V7.4. symbols. gmt" downloaded to run GSVA enrichment analyses from the Molecular Signatures Database (MSigDB), which ran by the "GSVA" R package [13].

2.6. Construction and validation of ARGs signatures and ARGs risk model

Initially, Applying the LASSO regression approach, we detected the most crucial survival-anoikis-related differentially expressed genes in OSC. Subsequently, the hub ARGs were selected via the multivariate regression method and subsequently utilized to establish the risk model. The risk score computation relies on the subsequent formula [14] (βi indicates the coefficients of each signature. Expi indicates the expression of each signature)

Risk scores $= \Sigma(\beta i \times \mathrm{Expi})$.

Using the median risk scores as the threshold, patients with OSC were divided into high-risk and low-risk groups. We conducted a survival analysis of OSC patients in the TCGA-OV and Test-set groups using Kaplan-Meier curves and log-rank statistical tests. Furthermore, we assessed the predictive capability of the ARGs.

2.7. Correlation of risk scores with immune infiltration

CIBERSORTx is a platform (accessible at https://cibersortx.stanford.edu) designed for estimating the abundance of 22 immune cell infiltrates in tumor samples [15]. We further performed a comparison of the proportions of immune infiltration and cell types in the high-risk and low-risk groups. The association between the risk score and the proportion of immune infiltration was analyzed using Spearman's correlation analysis.

2.8. Establishment and evaluation of a nomogram

The Univariate Cox regression method was applied to assess the significance of risk scores and clinical characteristics. (Age, grade, stage, residue size chemotherapy, radiotherapy, and neoplasm subdivision) on the prognosis of OSC patients. Statistically significant variables were incorporated in the multivariate Cox regression model to determine factors that influence OSC survival. Finally, a nomogram for predicting survival was constructed based on these independent influences. In addition, we utilized Decision Curve Analysis (DCA) and calibration curves for validating the precision of the signature model in both the TCGA-OV set and the test set.

2.9. Cell lines

SKOV3 is the human ovarian plasmacytoid cystic adenocarcinoma cell line that was used as the test group. IOSE80 is the human normal ovarian epithelial cell line that was the negative control group. PANC1 was used as the positive control group, representing the human pancreatic cancer cell line. And all cell lines were purchased by Shanghai Biological Company. IOSE80 cells were grown in DMEM high sugar medium, which is the mixture of 10% FBS and 1% penicillin-streptomycin; SKOV3, PANC1 cells were cultivated in McCoy's 5A medium, consisting of 10% FBS and 1% penicillin-streptomycin, and then incubated in a humidified CO2 incubator at 37 °C.

2.10. RT-PCR

Total intracellular RNA was isolated using TRIzol reagent, and cDNA was generated through reverse transcription for RT-PCR. Finally, PCR was performed using the designated kit. The amplification process involved pre-denaturation at 95 °C lasting 15 min, denaturation at 94 °C for 30 s, annealing for 30 s, extension at 72 °C for 30 s, and a total of 40 cycles. The primer sequences can be found in Table 1.

Table 1
RT-PCR primers used in this study.

Primer name	Primer type	Primer sequence (5′→3′)
GAPDH	Forward	GGAGCGAGATCCCTCCAAAAT
	Reverse	GGCTGTTGTCATACTTCTCATGG
ARHGEF7	Forward	TGCTTTCAACGTACCTACGGC
	Reverse	GGCAACTTGGTGCATTCTTCTAA
CCDC80	Forward	TCCCTGGAGAACTTCCTATCC
	Reverse	AGCAGAGATCACCAGCAACC
CASP2	Forward	GCAAACCTCAGGGAAACATT
	Reverse	TGTCGGCATACTGTTTCAGCA
PAK4	Forward	ATCTGGTCGCTGGGGATAATG
	Reverse	CAGGTTGTCCCGAATCATCTTC
SKP2	Forward	CACGGAAACGGCTGAAGA
	Reverse	AGCAACCGACCAGTCACAT
NOTCH4	Forward	CCAACCCTGCGATAATGCGAG
	Reverse	AGTCATCCGTTGAGACCCTGC

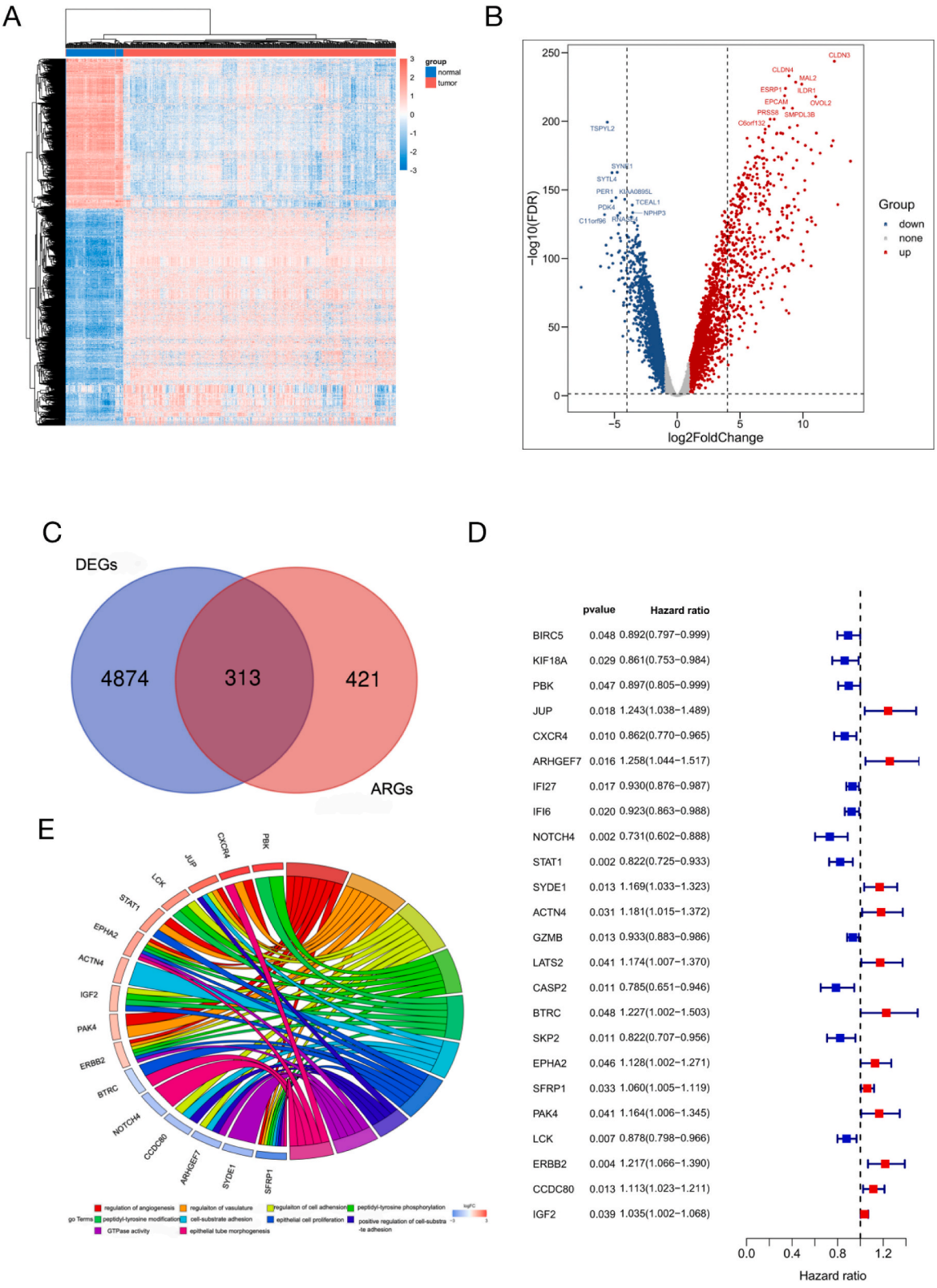

Fig. 1. Differences and characteristics of ARGs in OSC. (A) Heatmap and (B) volcano plot of gene expression in OSC and normal ovarian samples. (C) Differential expression of 313 ARGs in OSC and normal ovarian samples. (D) The forest plot suggested that 24 ARGs were associated with OSC prognosis. (E) The circle plot suggested GO analysis of 24 ARGs.

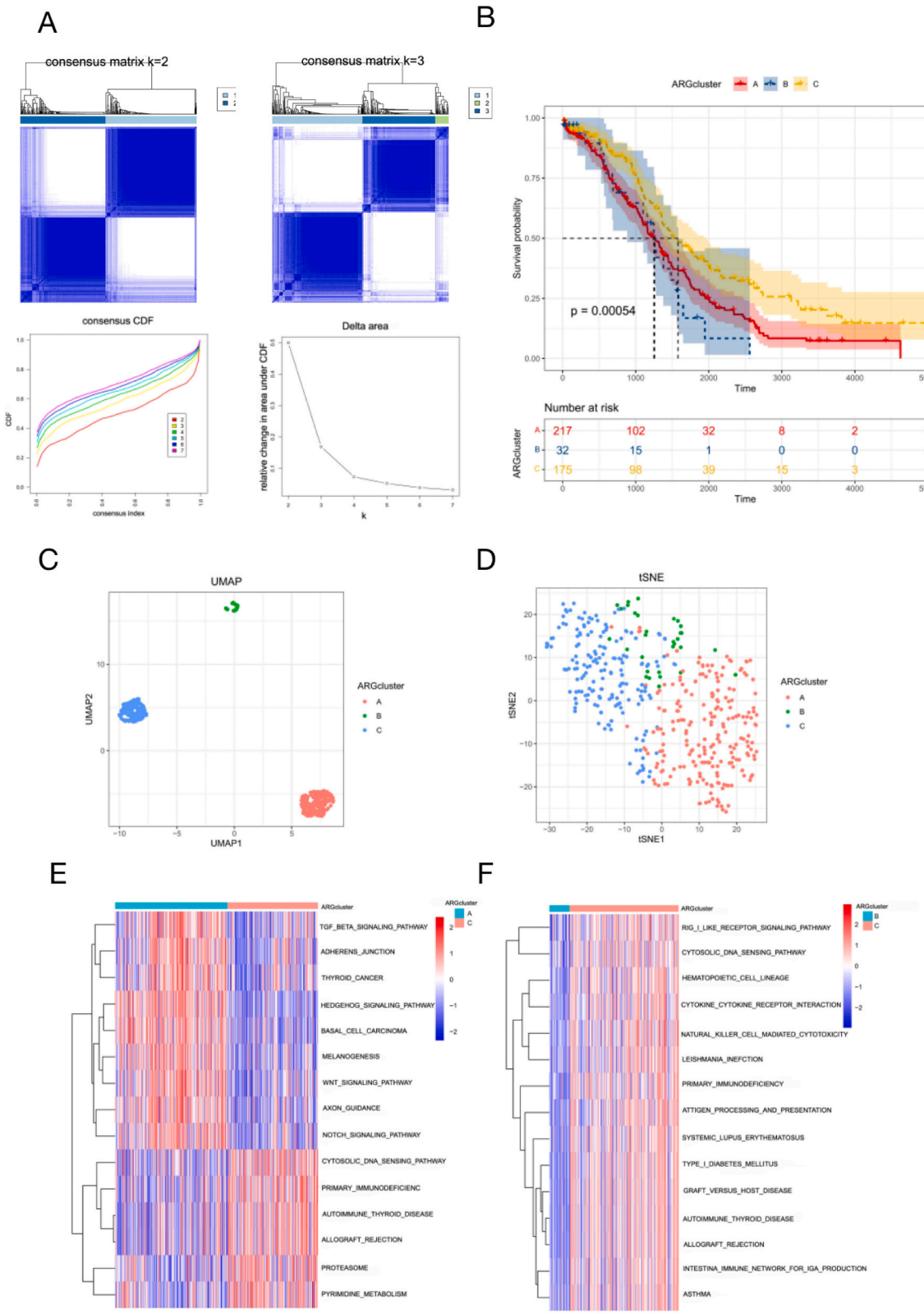

Fig. 2. Subtypes of OSC related by 24 ARGs. (A) The consensus matrix for k = 3 was derived by consensus clustering. (B) OS for three subtypes. (C) UMAP and (D) tSNE differentiate three subtypes. (E) GSVA analyses focused on KEGG differences between Cluster A and Cluster C. (F) GSVA analyses focused on KEGG differences between Cluster B and Cluster C.

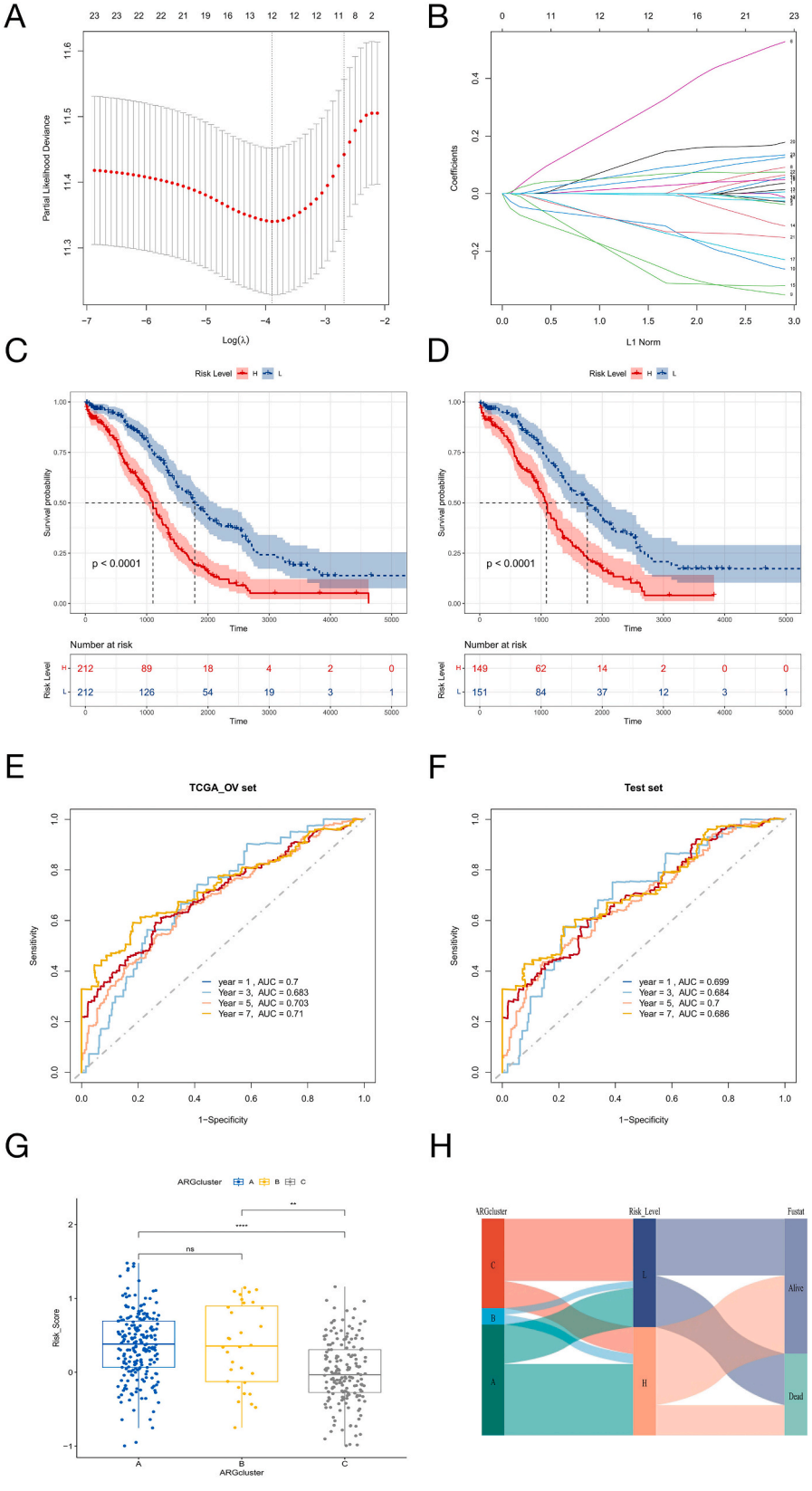

(caption on next page)

Fig. 3. Identify ARGs. (A) Lasso coefficient values were calculated regarding 24 ARGs in OSC. (B) The overview of Lasso coefficients. (C) OS of risk groups in TCGA OV set ($p < 0.0001$). (D) OS of risk groups in the Test set. (E, F) The ROC curves of OS at 1-, 3-, 5-, and 7-year intervals. (G) Risk score in 3 clusters. (H) The Sankey diagram demonstrates clusters, risk scores, and life status.

2.11. Statistical analysis

When examining differential genes between OSC and normal patients, An FDR q-value of <0.05 was considered to be a significant threshold. Group comparisons were conducted using the rank-sum test. For the analysis of overall survival (OS), OSC patients who passed away were defined as clinical endpoints and their survival time and outcomes were compared. The Kaplan-Meier method was utilized for calculating the survival rate of OSC patients, and the log-rank test was applied to compare the survival curves among the groups. Univariate Cox regression was performed to evaluate individual hazard ratios (HRs) for OS. HRs with 95% confidence intervals (CIs) were determined, assessing the hazard risks of individual factors. Variables with a significance level of $P < 0.05$ in univariate analyses were entered into multivariate analyses. The study was statistically analyzed using R software (version 4.2.1), and A P value < 0.05 was considered to indicate significance.

3. Results

3.1. Identification of ARGs associated with prognosis

After initial processing, there were 11,926 mRNA-expressing sequences in the TCGA-OSC cohort. We filtered 5187 DEGs with the "limma" R package, and the heatmap, as well as the volcano plot, showed upregulated and downregulated DEGs (Fig. 1A and B). We obtained 313 differentially expressed ARGs by intersecting DEGs with 734 ARGs on a Venn diagram (Fig. 1C). Subsequently, the univariate Cox regression analysis indicated that 24 ARGs showed significant associations with OSC prognosis. ($p < 0.05$). The forest plot revealed that there were 12 ARGs relevant to poor prognosis, such as NOTCH4, CASP2 SKP2, LCK, BIRC5, KIF18A, PBK, CXCR4, and IF127.IF16, STAT1, GZMB, and 12 additional ARGs were protective factors for OSC, such as JUP, ARHGEF7, BTRC, PAK4, CCDC80, SYDE1, ACTN4, LATS2, EPHA2, SFRP1, ERBB2, ICF2 (Fig. 1D). Our subsequent GO analysis demonstrated that the 24 identified ARGs were significantly linked to angiogenesis, vasculature development, and positive regulation of cell adhesion pathways. And the circle diagram showed a linkage between 24 ARGs and the top 10 pathways (Fig. 1E).

3.2. Classification of OSC into 3 subtypes based on 24 ARGs using consensus clustering

To explore the potential association between 24 survival-related ARGs and OSC, we attempted to analyze the subtypes of OSC using the "ConsensusClusterPlus" R package. Considering heatmap, CDF, and Delt area, the best clustering effect was when $k = 3$, OSC was divided into three subtypes (Fig. 2A). Fig. 2B showed that the prognosis of the three subtypes differed, with the best survival outcome in cluster C. ($P < 0.0001$). In Fig. 2C, D, Umap and tSNE revealed the high accuracy of the clustering analysis. To investigate the possible reasons for the excellent prognosis in cluster C, differences in the Kyoto Genome Encyclopedia (KEGG) pathway among clusters A, B and C were analyzed using the "GSVA" R package. We were surprised to find that cluster C was richer in immune-related pathways (Fig. 2E), for instance, rig_I_like receptor, antigen processing, natural killer cell-mediated cytotoxicity, presentation. By contrast, Clusters A and B exhibited a higher enrichment in pathogenic pathways, such as the proteasome pathway, TGF BETA, Hedgehog, WNT, and NOTCH (Fig. 2F).

3.3. Construction and validation of hub ARGs signatures and ARGs risk model

After performing univariate Cox regression analysis, we obtained 24 ARGs meaningfully associated with OSC survival outcomes. Then 12 ARGs were filtered by LASSO regression analysis (Fig. 3 A, B). Ultimately, the seven hub ARGs were identified through multivariate Cox regression analyses. ARHGEF7, PAK4, and CCDC80 independently influenced poor prognosis. while NOTCH4, CASP2, SKP2, and LCK were relevant to a good prognosis for OSC patients (Table 2). The risk score of ARGs was accordingly formulated as Risk Score = 0.403030211 × ARHGEF7 + (- 0.314885395) × NOTCH4 + (- 0.383007581) × CASP2 +(- 0.170540833) × SKP2 + 0.184375008 × PAK4 + (−0.161770924) × LCK + 0.113686217 × CCDC80. Since then, the ARGs risk model was

Table 2
Multivariable Cox regression of TCGA-OSC (N = 424).

	Coefficient	HR	95CI	*P*-value
ARHGEF7	0.403030211	1.50	1.19–1.88	<0.001
NOTCH4	−0.314885395	0.73	0.59–0.90	0.003
CASP2	−0.383007581	0.68	0.53–0.88	0.003
SKP2	−0.170540833	0.84	0.71–1.00	0.048
PAK4	0.184375008	1.20	1.02–1.41	0.026
LCK	−0.161770924	0.85	0.76–0.95	0.004
CCDC80	0.113686217	1.12	1.02–1.23	0.015

established by seven hub ARGs successfully. Based on the median risk scores, 424 OSC patients were categorized into 'high-risk' and 'low-risk' groups. It was clear to see that not only in the TCGA-OV set but also in the Test set low-risk OSC patients had significantly better survival outcomes (Fig. 3C and D). More importantly, the ROC curves indicated that the ARGs risk model provided excellent prediction for 1-, 3-, 5-, and 7-year survival in both OSC patient groups. (Fig. 3E and F). In addition, patients in cluster C with the best prognosis for OSC had the lowest risk scores (Fig. 3G). The Sankey diagram demonstrated the changes in ARGclusters, risk stratification, and life status of the OSC patients (Fig. 3H).

3.4. Establishment and evaluation of a nomogram for OSC

Taking into account the impact of clinical characteristics on OSC survival, we included some significant clinical characteristics in the establishment of the prognostic nomogram. We found that age, stage, residue size, chemotherapy, and risk score were statistically associated with outcomes in OSC, through univariate Cox regression method (Table 3). Moreover, they were put into multivariate Cox analysis to ascertain independent factors affecting the prognosis of OSC patients, factors which included risk score, age, residual size (>20 mm), and chemotherapy were used to establish a new nomogram for predicting prognosis in OSC (Fig. 4A). It was easy to see that a 52-year-old OSC patient with a residual size >20 mm received standardized post-operative chemotherapy with a risk score of −0.417 in Fig. 4B. Here, 1-, 3-, 5-, and 7-year survival rates were 95.4%, 78.3%, 52.7%, and 39%, respectively. Calibration plots showed nomogram had great predictive value in two sets (Fig. 4C and D). The 1- and 3-year DCA also indicated that a higher clinical benefit provided by the nomogram compared to the single ARGs risk model. (Fig. 4E and F).

3.5. Association between immune infiltration and risk score

The tumor immune microenvironment (TIME), a critical environment that regulates tumor development, infiltration, and metastasis, consists mainly of infiltrating immune cells, chemokines, and cytokines. CIBERSORTx analysis was utilized to assess the levels of 22 immune cell infiltrates in the ovarian tissue in 424 OSC patients. Trends in immune cell infiltration were observed by ranking OSC patients in descending order of risk score (Fig. 5 A). Fig. 5B and C have clearly shown that the infiltration of macrophage M0, macrophage M1, naive CD4 T cells, memory CD4 T cells and CD8 T cells was statistically significant within the risk groups. Risk score showed a negative correlation with macrophage M1 immune infiltration. ($r_s = -0.21, P < 0.05$) , but positively associated with resting memory CD4 T cells ($r_s = 0.21$, $P < 0.05$). The relevance between immune cells in OSC may provide insights to understand better the composition and interactions of the TIME. Fig. 5D suggested that Macrophages M1 may have synergistic effects with T cells CD8 and Plasma Cells in OSC.

3.6. Correlation between the ARGs signatures and immune infiltration

Fig. 6A showed that the seven ARGs genes have different patterns of expression between the normal and tumor groups. ARHGEF7, NOTCH, and CCDC80 were down-regulated in OSC, while CASP2, LCK, PAK4, and SKP2 were up-regulated in OSC. Fig. 6B showed that CCDC80 and LCK were the primary ARGs involved in immune infiltration, mainly in CD8 T cells, Macrophages M1, and Macrophages M2. What's more, e used the GDSC database to predict the drug sensitivity responses. A significant variation in the half-maximal inhibitory concentration (IC50) for 70 drugs was found between the two risk groups. (Supplementary Fig. S1).

3.7. The RT-PCR results of three tumor-promoting ARGs in cell lines

We examined the expression of seven hub ARGs in cell lines by RT-PCR. The results revealed that ARHGEF7 and CCDC80 were expressed in SKOV3 and PANC1 cell lines at lower levels than in the IOSE80 cell line. (Fig. 7A, G). Instead, the expression of NOTCH4, CASP2, SKP2, PAK4, and LCK were significantly higher in SKOV3 and PANC1 than in IOSE80 cell lines (Fig. 7B–F). Comparison of the PCR results with the bioinformatic analysis of the public sequencing data, and the agreement was 6/7, with a match rate of 85.7%.

4. Discussion

Multiple signaling pathways contribute to anoikis resistance in OSC, emphasizing the significance of targeting associated genes to

Table 3
Univariate Cox regression of TCGA-OSC (N = 424).

	HR	HR.95L	HR.95H	*P*-value
Age	1.021	1.009	1.032	<0.0001
Grade	1.186	0.835	1.687	0.3
Stage	1.333	1.020	1.74	0.04
Residue.size	1.314	1.159	1.489	<0.0001
Chemotherapy	0.2612	0.156	0.436	<0.0001
Radiotherapy	0.7757	0.491	1.228	0.3
Neoplasm subdivision	1.019	0.769	1.352	0.9
Risk Score	3.135	2.359	4.165	<0.0001

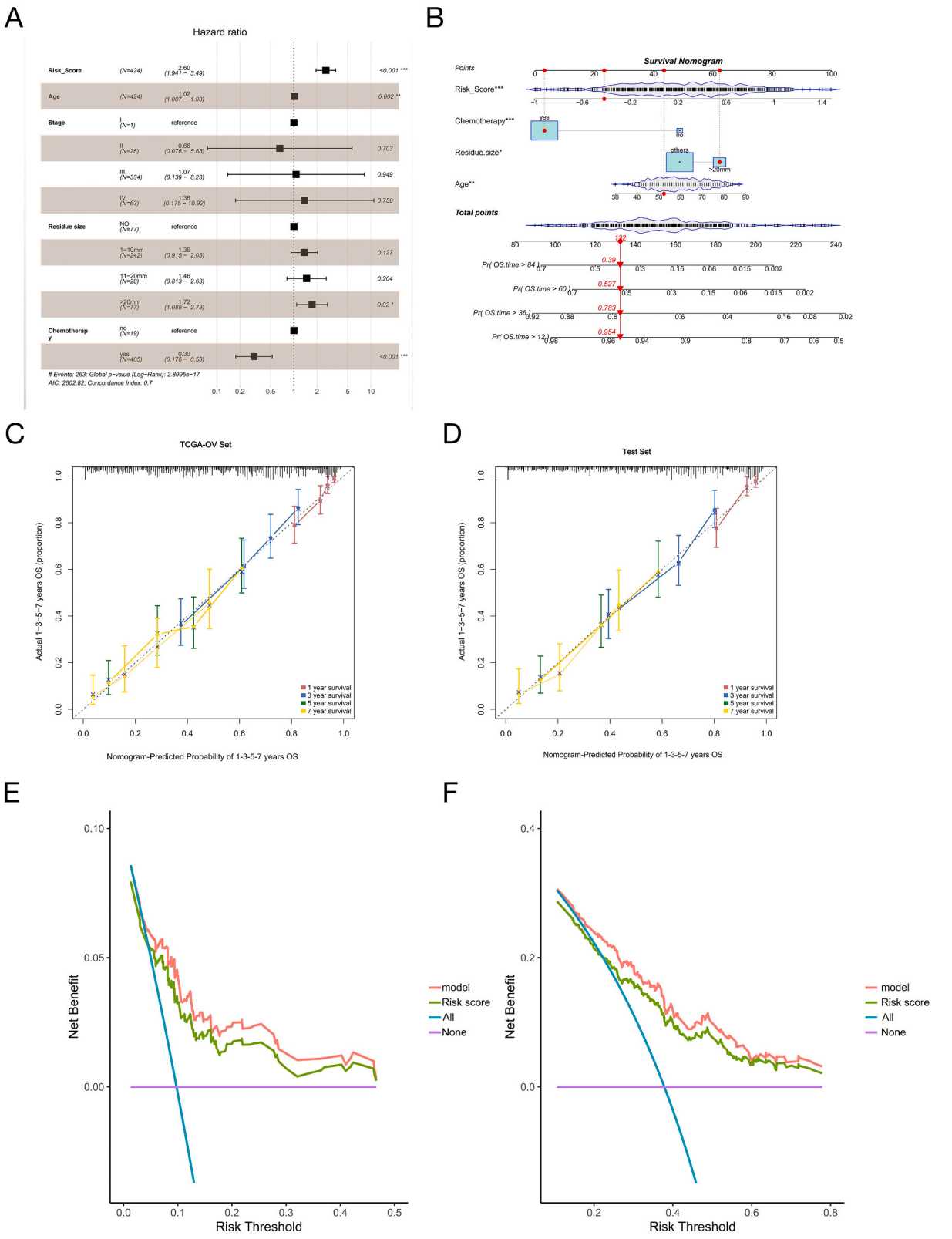

ig. 4. Establishment and validation of prognostic nomogram. (A) Multivariate Cox regression forest plot of risk scores and clinical features in OSC patients. (B) Nomogram plot. (C, D) Calibration plot for the nomogram in TCGA OV set and Test set. (E, F) DCA curves of the nomogram and risk score for 1-,3-year OS in OSC.

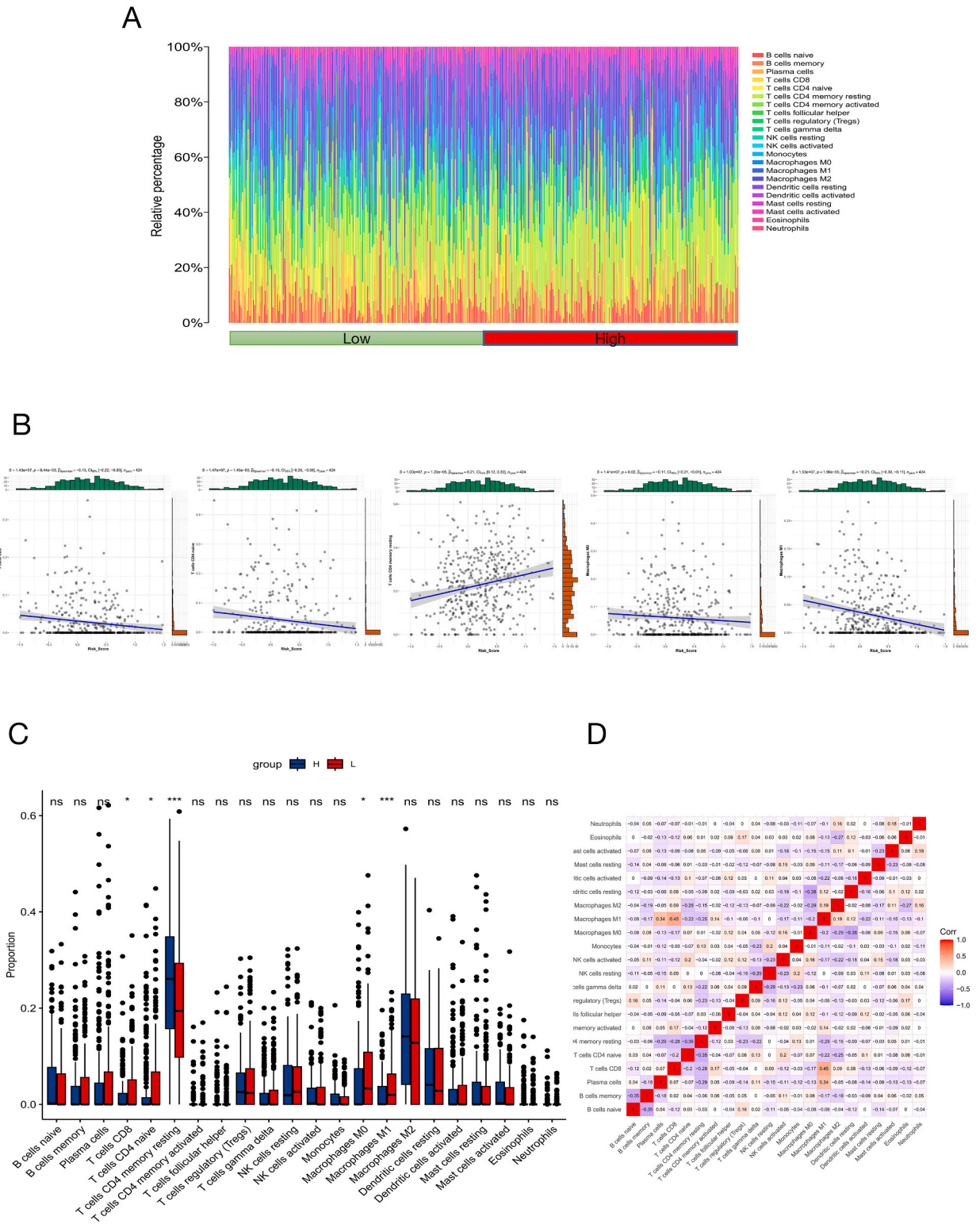

Fig. 5. Immunological microenvironment of OSC in risk groups. (A) Proportions of infiltrating immune cells in 424 OSC patients. (B) Correlation analysis between risk scores and the abundance of five immune cells. (C) Disparities in immune infiltrate proportions between risk groups.(D) Correlation among 22 immune cell types.

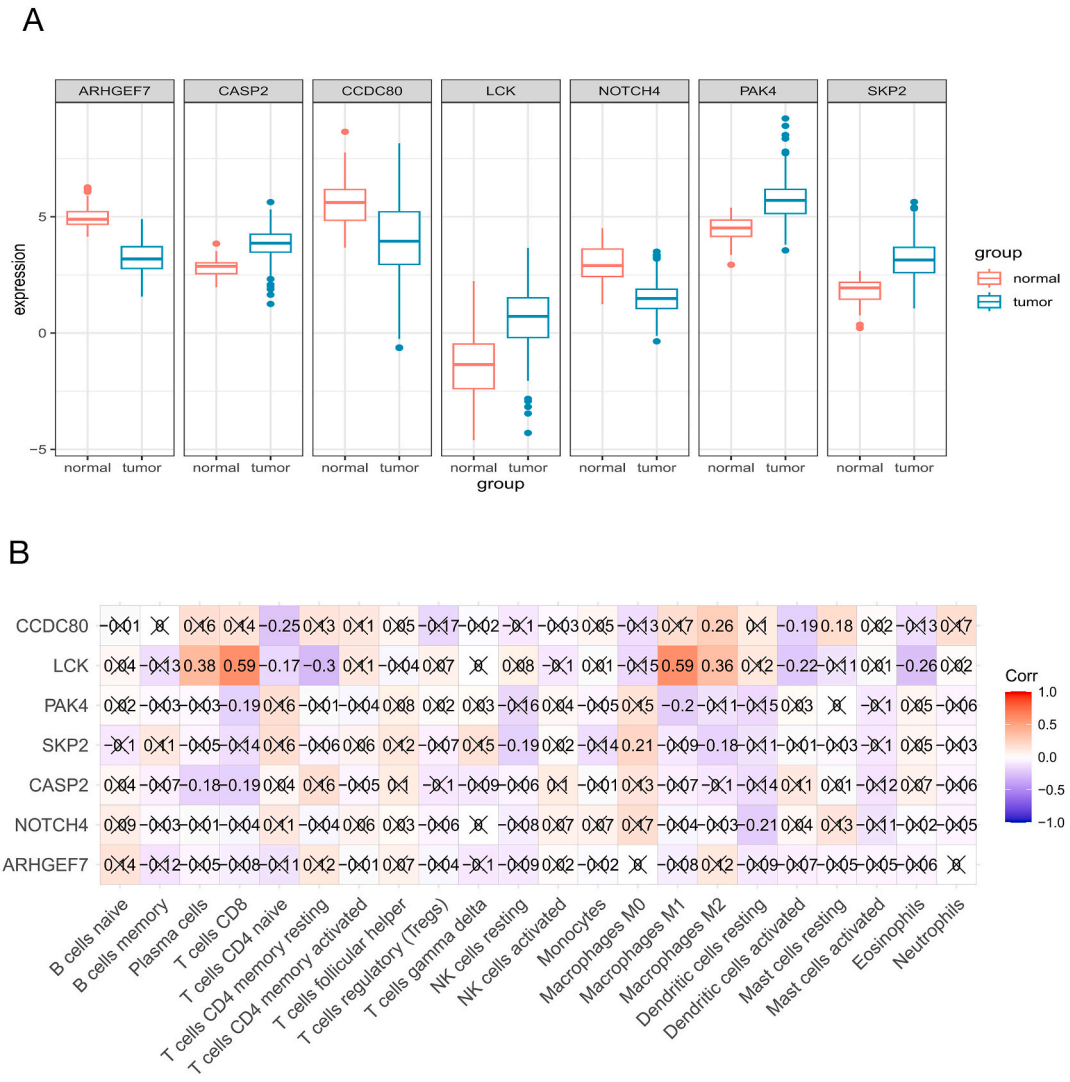

Fig. 6. Association between immune infiltration and ARGs signatures. (A)The box plots depict the expression patterns of seven hub genes. (B) Association among seven hub genes and 22 Immune cells.

combat OSC progression and metastasis [16]. Multigene analyses reflect the complex interactions among the various parameters that influence antitumor resistance in tumor pathology. Therefore, this multigene approach can be used in characterizing tumor biology and supporting clinical decision-making.

Seven hub ARGs were identified, and risk models were successfully constructed during this research, of which ARHGEF7, NOTCH, and CCDC80 were down-regulated in OSC, while CASP2, LCK, PAK4, and SKP2 were up-regulated in OSC. A review of the reports revealed that these genes are critical molecules in several tumors' development, progression, and metastasis. ARHGEF7 was relevant to cytoskeletal remodeling [17]. In colorectal adenocarcinoma, high ARHGEF7 expression was an independent risk factor impacting overall survival (OS) and disease-free survival (DFS). It was significantly associated with distant metastasis from lymph nodes and mesentery [18,19]. CASP2 is a cysteine protease family member. Reports have shown that CASP2 exhibits tumor-suppressive effects [20]. SKP2 is a type of F-box protein. Studies have reported that up-regulated SKP2 is one of the critical targets for tumor therapy, which affects tumor formation, metastasis, cell cycle development, and cellular senescence [21,22]. PAK4 is a typical class II representative within the PAK family. It reports that PAK4 is amplified and overexpressed in various tumors, such as bladder cancer and osteosarcoma, and is considered one of the key factors in tumor cell signaling [23,24]. LCK, also known as T-lymphocyte tyrosine kinase, is essential for forming effector T cells and T cell-mediated immune responses. In cholangiocarcinoma, LCK regulates YAP tyrosine phosphorylation and nuclear localization to promote tumor development, and its expression level is associated with early tumor recurrence [25]. T The CCDC80 (DRO1) is lowly expressed in the thyroid, papillary, pancreatic, and colon cancer cell lines [26]. Recent research has revealed that CCDC80 is a tumor suppressor in the tumor microenvironment [27]. The Notch signaling pathway is an evolutionarily conserved mechanism crucial for fetal development, organ formation, and tissue homeostasis. NOTCH4 is a NOTCH

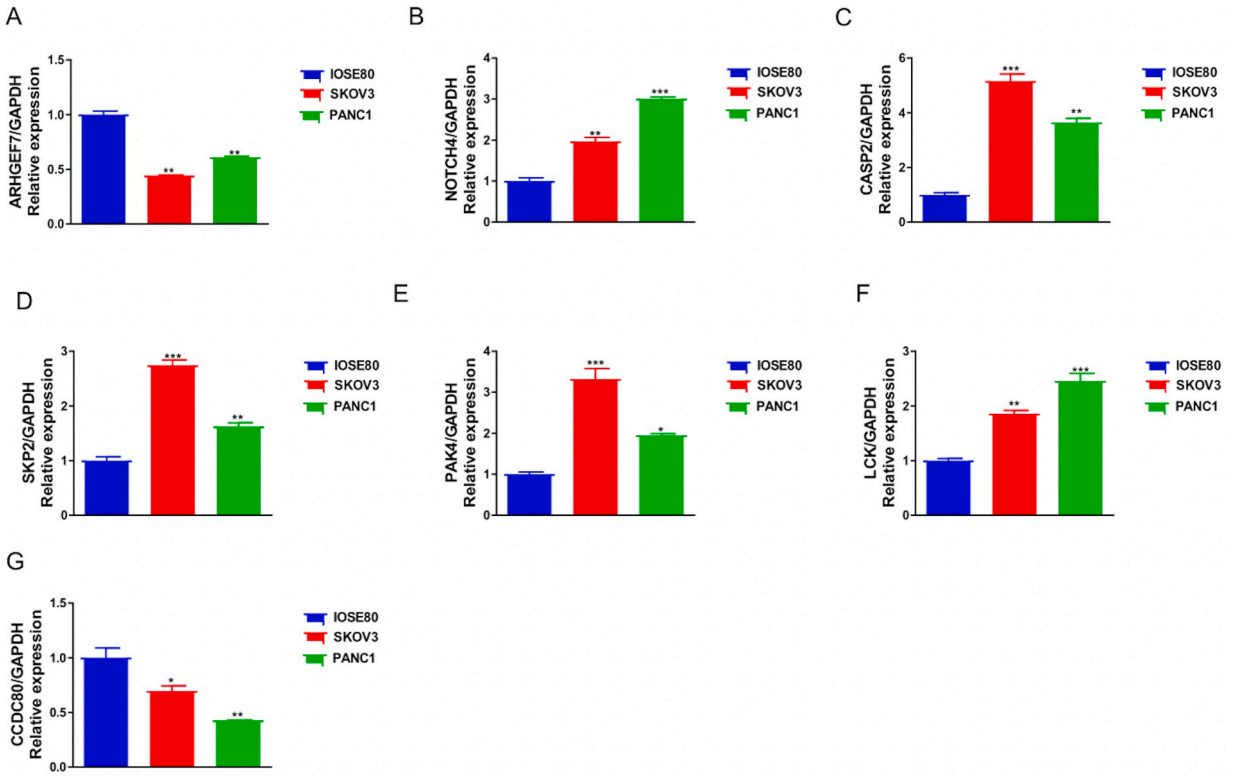

Fig. 7. Results of RT-PCR. The expression of ARHGEF7 (A), NOTCH4 (B), CASP2 (C), SKP2 (D), PAK4 (E), LCK (F), and CCDC80(G) in the three cell lines. $*p < 0.05$, $**p < 0.01$, $***p < 0.001$.

family member whose precise role in tumorigenesis and development is not yet clear [28]. In combination with these reports, the seven hub ARGs in our study could take a typical role in OSC development, progression, and metastasis. To our confusion, we found that NOTCH4 was lowly expressed in OSC tissue samples in the TCGA database, while RT-PCR results in SKOV3 cell lines were highly expressed. Similarly, the expression pattern of NOTCH4 mRNA was reported to be reversed in tissue samples and cell lines from non-small cell lung cancer [29,30], and hepatocellular carcinoma [31]. We suspect that there may be several following reasons for this. Given that sequencing and PCR are two different assays, it is customary and reasonable that a certain degree of inconsistency (about 30–40%) will occur [32]. In addition to this, some studies have found Notch4 exerts oncogenic or oncostatic effects, often depending on the tissue microenvironment, gene expression, and immune infiltration [29,33], However, In certain instances, different Notch receptors may lead to contradictory outcomes or influence the clinical characteristics and advancement of specific tumors [34,35]. The influence of the tumor microenvironment on NOTCH4 expression in tissue samples of different pathological grades from OSC patients in TCGA is not negligible. Consequently, further studies based on larger samples and different biological levels are needed to investigate the mysteries of NOTCH4 and tumors. With a more comprehensive understanding of the variances in biological characteristics within distinct microenvironments and subtypes, the role of NOTCH4 in OSC is anticipated to be better elucidated.

In the current investigation, we effectively constructed a novel ARGs signature to forecast the prognosis of OSC patients. In addition, there is growing evidence showing that TME performs an invaluable function in supporting tumor growth, invasion and protecting tumors from host immune killing [36,37]. Therefore, we discussed the possible impact of immune activity on OSC on the basis of the ARGs risk model. The CIBERSORTx analysis demonstrated a negative association between the risk score and macrophage M1, but a positive correlation with resting memory CD4 T cells. Tumor-associated macrophages (TAMs) can be classified as anti-tumour M1 and pro-tumour M2 [38]. M2 releases various soluble factors (TNF-α, IL-6, TGF-β, CCL18, MMPs) responsible for activating multiple pathways in ovarian cancer cells to stimulate viability, proliferation, metastasis, as well as aggression [39], while impairing the immune cell activity, causing immune escape of ovarian cancer cells [40,41] which is one of the factors leading to drug resistance and poor survival in ovarian cancer [42]. Macrophages M1 can also co-exist in the TME of early-stage ovarian cancer, promoting anti-tumor immunity and acting in immunosurveillance [43]. Previous studies have shown that in non-small cell lung, hepatocellular carcinomas, and colorectal, increased infiltration density of Macrophages M1 and elevated M1/M2 ratios were positively associated with 5-year survival in tumor patients [44,45]. The result was also confirmed in ovarian cancer by Zhang et al. [46]. Garrido-Martin identified that compared to poor prognosis in M1 low-infiltrating tumors, M1 high-infiltrating tumors had a prognosis associated with high infiltration of $CD8^+$ T cells [47]. This is in accordance with our findings that the proportion of M1 infiltration was associated negatively with the risk score but positively with $CD8^+$ T cells. It indicated that highly infiltrated M1 and $CD8^+$ T cells inhibit anoikis resistance and suppress distant migration of OSC. Besides that, LCK had the highest coefficients of relevance to M1 and

$CD8^+$ T-cell infiltration in ARGs, and M1/CD8+ T-cells/LCK appears to be an attractive molecular pathway.

Despite our ARGs risk model and the nomogram constructed having superior predictive performance, it still requires a larger sample size to verify gene expression and to calibrate the prediction model and large multicenter clinical trials to validate the predictive models. And the potential mechanisms between anoikis genes and immune cells in OSC require additional in vivo and in vitro analysis.

In a word, this research effectively identified and validated the ARGs signature of OSC, our ARGs risk model can well predict the outcomes with OSC patients, and a nomogram can help predict physicians develop precision medicine in OSC and further investigate the immune landscape between different risk classifications, which will facilitate individualized treatment of OSC patients.

Author contribution statement

Yu-Ting Zhu: Conceived and designed the experiments; Performed the experiments; Analyzed and interpreted the data; Wrote the paper.

Shuang-Yue Wu; Yang Song; Jie Ying; Lu Tian: Analyzed and interpreted the data.

Hong-Liang Xu; He-Ping Zhang; Hui Yao; Wei-Yu Zhang; Qin-Qin Jin; Yin-Ting Yang; Xi-Ya Jiang; Nan Zhang; Shun Yao: Contributed reagents, materials, analysis tools or data.

Shu-Guang Zhou; Guo Chen: Conceived and designed the experiments; Wrote the paper.

Data availability statement

Data will be made available on request.

Ethics approval and consent to participate

Not applicable.

Declaration of competing interest

The authors declare that they have no known competing financial interests or personal relationships that could have appeared to influence the work reported in this paper.

Acknowledgments

This study was supported by the Research Fund Project of Anhui Medical University (Grant ID: 2020xkj236), the Natural Science Foundation of Higher Education Institutions of Anhui Province (Grant ID: KJ2021A0352), the Research Project of Anhui Province (Grant ID: 9001001875), and the Anhui Provincial Department of Science and Technology (Grant ID: 202204295107020048).

Appendix A. Supplementary data

Supplementary data to this article can be found online at https://doi.org/10.1016/j.heliyon.2023.e18708.

References

[1] R.L. Siegel, K.D. Miller, A. Jemal, Cancer statistics, 2020, CA A Cancer J. Clin. 70 (1) (2020) 7–30, https://doi.org/10.3322/caac.21590.
[2] R. Salani, F.J. Backes, M.F. Fung, et al., Posttreatment surveillance and diagnosis of recurrence in women with gynecologic malignancies: society of Gynecologic Oncologists recommendations, Am. J. Obstet. Gynecol. 204 (6) (2011) 466–478, https://doi.org/10.1016/j.ajog.2011.03.008.
[3] H. Sung, J. Ferlay, R.L. Siegel, et al., Global cancer statistics 2020: GLOBOCAN estimates of incidence and mortality worldwide for 36 cancers in 185 countries, CA A Cancer J. Clin. 71 (3) (2021) 209–2024 9, https://doi.org/10.3322/caac.21660.
[4] U.A. Matulonis, Management of newly diagnosed or recurrent ovarian cancer, Clin. Adv. Hematol. Oncol. 16 (6) (2018) 426–437.
[5] J.G. Nirmala, M. Lopus, Cell death mechanisms in eukaryotes, Cell Biol. Toxicol. 36 (2) (2020) 145–164, https://doi.org/10.1007/s10565-019-09496-2.
[6] H.J. Han, J.Y. Sung, S.H. Kim, et al., Fibronectin regulates anoikis resistance via cell aggregate formation, Cancer Lett. 508 (2021) 59–72, https://doi.org/10.1016/j.canlet.2021.03.011.
[7] H.F. Zhang, C.S. Hughes, W. Li, et al., Proteomic screens for suppressors of anoikis identify IL1RAP as a promising surface target in ewing sarcoma, Cancer Discov. 11 (11) (2021) 2884–2903, https://doi.org/10.1158/2159-8290.CD-20-1690.
[8] L. Jin, J. Chun, C. Pan, et al., The PLAG1-GDH1 Axis promotes anoikis resistance and tumor metastasis through CamKK2-AMPK signaling in LKB1-deficient lung cancer, Mol. Cell 69 (1) (2018) 87–99, https://doi.org/10.1016/j.molcel.2017.11.025.
[9] P. Gupta, N. Gupta, N.M. Fofaria, A. Ranjan, S.K. Srivastava, HER2-mediated GLI2 stabilization promotes anoikis resistance and metastasis of breast cancer cells, Cancer Lett. 442 (2019) 68–81, https://doi.org/10.1016/j.canlet.2018.10.021.
[10] W. Wang, X.B. Shen, D.B. Huang, W. Jia, W.B. Liu, Y.F. He, Peroxiredoxin 4 suppresses anoikis and augments growth and metastasis of hepatocellular carcinoma cells through the β-catenin/ID2 pathway, Cell. Oncol. 42 (6) (2019) 769–781, https://doi.org/10.1007/s13402-019-00460-0.
[11] J. Wang, Z. Luo, L. Lin, et al., Anoikis-associated lung cancer metastasis: mechanisms and therapies, 2022 Sep. 30, Cancers 14 (19) (2022) 4791, https://doi.org/10.3390/cancers14194791.

[12] M.D. Wilkerson, D.N. Hayes, ConsensusClusterPlus: a class discovery tool with confidence assessments and item tracking, Bioinformatics 26 (12) (2010) 1572–1573, https://doi.org/10.1093/bioinformatics/btq170.
[13] S. Hänzelmann, R. Castelo, J. Guinney, GSVA: gene set variation analysis for microarray and RNA-seq data, BMC Bioinf. 14 (2013) 7, https://doi.org/10.1186/1471-2105-14-7.
[14] Weiyu Zhang, Wujun Cao, Zhuting Tong, et al., Identification and validation of a novel necroptosis-related prognostic signature in cervical squamous cell carcinoma and endocervical adenocarcinoma [J], 1011000, Front. Oncol. 12 (2022) 1–17, https://doi.org/10.3389/fonc.2022.1011000.
[15] A.M. Newman, C.B. Steen, C.L. Liu, et al., Determining cell type abundance and expression from bulk tissues with digital cytometry, Nat. Biotechnol. 37 (7) (2019) 773–782, https://doi.org/10.1038/s41587-019-0114-2.
[16] B.T. Sawyer, L. Qamar, T.M. Yamamoto, et al., Targeting fatty acid oxidation to promote anoikis and inhibit ovarian cancer progression, Mol. Cancer Res. 18 (7) (2020) 1088–1098, https://doi.org/10.1158/1541-7786.MCR-19-1057.
[17] X. Lei, L. Deng, D. Liu, et al., ARHGEF7 promotes metastasis of colorectal adenocarcinoma by regulating the motility of cancer cells, Int. J. Oncol. 53 (5) (2018) 1980–1996, https://doi.org/10.3892/ijo.2018.4535.
[18] H. Ito, T. Tsunoda, M. Riku, et al., Indispensable role of STIL in the regulation of cancer cell motility through the lamellipodial accumulation of ARHGEF7-PAK1 complex, Oncogene 39 (9) (2020) 1931–1943, https://doi.org/10.1038/s41388-019-1115-9.
[19] C.D. Lawson, A.J. Ridley, Rho GTPase signaling complexes in cell migration and invasion, J. Cell Biol. 217 (2) (2018 Feb 5) 447–457, https://doi.org/10.1083/jcb.201612069.
[20] C. López-García, L. Sansregret, E. Domingo, et al., BCL9L dysfunction impairs caspase-2 expression permitting aneuploidy tolerance in colorectal cancer, Cancer Cell 31 (1) (2017) 79–93, https://doi.org/10.1016/j.ccell.2016.11.001.
[21] L.L. Thompson, A.K. Baergen, Z. Lichtensztejn, K.J. McManus, Reduced SKP1 expression induces chromosome instability through aberrant cyclin E1 protein turnover, Cancers 12 (3) (2020) 531, https://doi.org/10.3390/cancers12030531.
[22] S. Han, R. Wang, Y. Zhang, et al., The role of ubiquitination and deubiquitination in tumor invasion and metastasis, Int. J. Biol. Sci. 18 (6) (2022) 2292–2303, https://doi.org/10.7150/ijbs.69411.
[23] D.S. Chandrashekar, B.V.S.K. Chakravarthi, A.D. Robinson, et al., Therapeutically actionable PAK4 is amplified, overexpressed, and involved in bladder cancer progression, Oncogene 39 (20) (2020) 4077–4091, https://doi.org/10.1038/s41388-020-1275-7.
[24] Z.F. Li, Y.D. Yao, Y.Y. Zhao, et al., Effects of PAK4/LIMK1/Cofilin-1 signaling pathway on proliferation, invasion, and migration of human osteosarcoma cells, J. Clin. Lab. Anal. 34 (9) (2020), e23362, https://doi.org/10.1002/jcla.23362.
[25] T. Sugihara, N.W. Werneburg, M.C. Hernandez, et al., YAP tyrosine phosphorylation and nuclear localization in cholangiocarcinoma cells are regulated by LCK and independent of LATS activity, Mol. Cancer Res. 16 (10) (2018) 1556–1567, https://doi.org/10.1158/1541-7786.MCR-18-0158.
[26] A. Ferraro, F. Schepis, V. Leone, et al., Tumor suppressor role of the CL2/DRO1/CCDC80 gene in thyroid carcinogenesis, J. Clin. Endocrinol. Metab. 98 (7) (2013) 2834–2843, https://doi.org/10.1210/jc.2012-2926.
[27] J.I. Christian, A. Pastula, A. Herbst, et al., Loss of DRO1/CCDC80 in the tumor microenvironment promotes carcinogenesis, Oncotarget 13 (2022) 615–627, https://doi.org/10.18632/oncotarget.28084.
[28] M. Katoh, M. Katoh, Precision medicine for human cancers with Notch signaling dysregulation (Review), Int. J. Mol. Med. 45 (2) (2020) 279–297, https://doi.org/10.3892/ijmm.2019.4418.
[29] Y. Qing, Y. Wang, C. Hu, et al., Evaluation of NOTCH family genes' expression and prognostic value in prostate cancer, Transl. Androl. Urol. 11 (5) (2022) 627–642, https://doi.org/10.21037/tau-22-281.
[30] Y. Wang, R. Yang, X. Wang, et al., Evaluation of the correlation of vasculogenic mimicry, Notch4, DLL4, and KAI1/CD82 in the prediction of metastasis and prognosis in non-small cell lung cancer, Medicine (Baltim.) 97 (52) (2018), e13817, https://doi.org/10.1097/MD.0000000000013817.
[31] L. Gramantieri, C. Giovannini, A. Lanzi, et al., Aberrant Notch3 and Notch4 expression in human hepatocellular carcinoma, Liver Int. 27 (7) (2007) 997–1007, https://doi.org/10.1111/j.1478-3231.2007.01544.x.
[32] SEQC/MAQC-III Consortium, A comprehensive assessment of RNA-seq accuracy, reproducibility, and information content by the Sequencing Quality Control Consortium, Nat. Biotechnol. 32 (9) (2014) 903–914, https://doi.org/10.1038/nbt.2957.
[33] A.K. Biktasova, D.F. Dudimah, R.V. Uzhachenko, et al., Multivalent forms of the Notch ligand DLL-1 enhance antitumor T-cell immunity in lung cancer and improve efficacy of EGFR-targeted therapy, Cancer Res. 75 (22) (2015) 4728–4741, https://doi.org/10.1158/0008-5472.CAN-14-1154.
[34] D. Bellavia, S. Checquolo, A.F. Campese, et al., Notch3: from subtle structural differences to functional diversity, Oncogene 27 (38) (2008 Sep 1) 5092–5098, https://doi.org/10.1038/onc.2008.230.
[35] E. Bonyadi Rad, H. Hammerlindl, C. Wels, et al., Notch4 signaling induces a mesenchymal-epithelial-like transition in melanoma cells to suppress malignant behaviors, Cancer Res. 76 (7) (2016) 1690–1697, https://doi.org/10.1158/0008-5472.CAN-15-1722.
[36] S. Xing, K. Hu, Y. Wang, Tumor immune microenvironment and immunotherapy in non-small cell lung cancer: update and new challenges, 2022 Dec 1, Aging Dis. 13 (6) (2022) 1615–1632, https://doi.org/10.14336/AD.2022.0407.
[37] L. Yang, G. Liu, Y. Li, Y. Pan, The emergence of tumor-infiltrating lymphocytes in nasopharyngeal carcinoma: predictive value and immunotherapy implications, Genes Dis. 9 (5) (2021) 1208–1219, https://doi.org/10.1016/j.gendis.2021.07.002. Published 2021 Aug 8.
[38] B.Z. Qian, J.W. Pollard, Macrophage diversity enhances tumor progression and metastasis, Cell 141 (1) (2010) 39–51, https://doi.org/10.1016/j.cell.2010.03.014.
[39] T. Adhikary, A. Wortmann, F. Finkernagel, S. Lieber, A. Nist, T. Stiewe, U. Wagner, S. Müller-Brüsselbach, S. Reinartz, R. Müller, Interferon signaling in ascites-associated macrophages is linked to a favorable clinical outcome in a subgroup of ovarian carcinoma patients, BMC Genom. 18 (1) (2017 Mar 21) 243, https://doi.org/10.1186/s12864-017-3630-9.
[40] K.K. Goswami, T. Ghosh, S. Ghosh, M. Sarkar, A. Bose, R. Baral, Tumor promoting role of anti-tumor macrophages in tumor microenvironment, Jun, Cell. Immunol. 316 (2017) 1–10, https://doi.org/10.1016/j.cellimm.2017.04.005.
[41] E.K. Colvin, Tumor-associated macrophages contribute to tumor progression in ovarian cancer, Front. Oncol. 4 (2014 Jun 6) 137, https://doi.org/10.3389/fonc.2014.00137.
[42] Z. Yafei, G. Jun, G. Guolan, Correlation between macrophage infiltration and prognosis of ovarian cancer—a preliminary study, Biomed. Res. 27 (2016).
[43] L. Cao, X. Che, X. Qiu, et al., M2 macrophage infiltration into tumor islets leads to poor prognosis in non-small-cell lung cancer, Cancer Manag. Res. 11 (2019) 6125–6138, https://doi.org/10.2147/CMAR.S199832.
[44] Y. Wu, L. Yuan, Q. Lu, H. Xu, X. He, Distinctive profiles of tumor-infiltrating immune cells and association with intensity of infiltration in colorectal cancer, Oncol. Lett. 15 (3) (2018) 3876–3882, https://doi.org/10.3892/ol.2018.7771.
[45] K. Minami, K. Hiwatashi, S. Ueno, et al., Prognostic significance of CD68, CD163 and Folate receptor-β positive macrophages in hepatocellular carcinoma, Exp. Ther. Med. 15 (5) (2018) 4465–4476, https://doi.org/10.3892/etm.2018.5959.
[46] M. Zhang, Y. He, X. Sun, et al., A high M1/M2 ratio of tumor-associated macrophages is associated with extended survival in ovarian cancer patients, J. Ovarian Res. 7 (2014) 19, https://doi.org/10.1186/1757-2215-7-19.
[47] E.M. Garrido-Martin, T.W.P. Mellows, J. Clarke, et al., M1hot tumor-associated macrophages boost tissue-resident memory T cells infiltration and survival in human lung cancer, J. Immunother. Canc. 8 (2) (2020), e000778, https://doi.org/10.1136/jitc-2020-000778.